Pitch Angle Isotropy of Relativistic Electron Microbursts as Observed by SAMPEX/HILT: Statistical and Storm-time Properties

College of Arts and Sciences Honors Thesis

Department of Astrophysical & Planetary Sciences

Defense Date: March 29, 2022

Conrad Meyer-Reed

Honors thesis committee:
Dr. Lauren Blum (Thesis Advisor)
Department of Astrophysical & Planetary Sciences, CU Boulder
Dr. Ann-Marie Madigan
Department of Astrophysical & Planetary Sciences, CU Boulder
Dr. Kate Fischer
Arts and Sciences Honors Residential Academic Program, CU Boulder

Pitch Angle Isotropy of Relativistic Electron Microbursts as Observed by SAMPEX/HILT: Statistical and Storm-time Properties

Conrad Meyer-Reed,[1,2] Lauren Blum,[1,2] and Mykhaylo Shumko[3]

[1] University of Colorado Boulder
[2] Laboratory for Atmospheric and Space Physics
[3] NASA Goddard Space Flight Center

ABSTRACT

Observations of relativistic electron precipitation events from Earth's inner magnetosphere to the upper atmosphere have provided essential information about the source/loss processes and dynamics of Earth's radiation belts. This study discusses electron microbursts, which are ~100 millisecond duration streams of MeV-energy electrons often observed at high latitudes. By drawing correlations between measurements from the Heavy Ion Large Telescope (HILT) instrument onboard the Solar, Anomalous, and Magnetospheric Particle Explorer (SAMPEX) satellite and its temporal and spatial data, we quantify the effects of these microburst events on electron loss rates at different regions within the the Earth's magnetosphere. Additionally, we conduct a storm-time analysis of microburst characteristics using ground-based measurements of geomagnetic storm activity. Equatorial electron pitch angle isotropy is one such indicator of electron precipitation into the atmosphere, with isotropic populations resulting in a full bounce loss cone (BLC) and anisotropic populations resulting in an empty BLC. Results from this study have shown that high flux magnitude microbursts typically scatter electron pitch angles into the BLC more than low flux magnitude microbursts. This study has also found that microbursts are more isotropic than the background population in the morning, evening, and midnight local times and more similar in anisotropy to the background population in the noon local times. Furthermore, the results of this study show that microbursts are most effective at scattering electron pitch angles during the initial and main phases of intense geomagnetic storms.

1. INTRODUCTION

The Van Allen radiation belts are clouds of electrons and ions transferred from the interplanetary magnetic field into Earth's global magnetic field, which acts as a protective shield preventing solar wind from stripping Earth's atmosphere. During geomagnetic storms, the changing magnetic field strengths in the magnetosphere cause rapid changes in plasma densities. This results in near-Earth space weather events that cause GPS signal error, damage spacecraft equipment, and blackout ground-based power grids. If the source and loss processes of electrons in the radiation belts are better understood, we can mitigate the effects of potentially harmful space weather events by designing space missions and ground infrastructure using information about when and where charged particle fluxes related to geomagnetic storm activity are the highest.

Earth's radiation belts are composed of relativistic electrons moving in 3 primary motions, shown in Figure 1a. On the smallest scale, the Lorentz force causes electron gyro motion around the local magnetic field lines of Earth's dipole magnetic field. This motion happens on the timescale of milliseconds. The second motion is called bounce motion, which causes electrons to travel longitudinally along the local magnetic field lines bouncing periodically from the upper hemisphere to the lower hemisphere in the radiation belts on a timescale of seconds. Electron bounce motion is caused by the Lorentz force in a magnetic bottle like Earth's magnetic field. The effects of the Lorentz force on a charged particle can be seen in Figure 1b. Lastly, drift motion is the latitudinal motion of electrons around the Earth caused by a differential in magnetic field strength along electron gyro paths. Electron drift motion occurs on the timescale of minutes.

In this study, we look at relativistic electron precipitation which is related to electron bounce motion. During a bounce cycle, the location at which an electron reverses direction and travels back toward the equatorial region is called the mirror point. At the mirror point, the pitch angle of an electron is perpendicular to the local magnetic
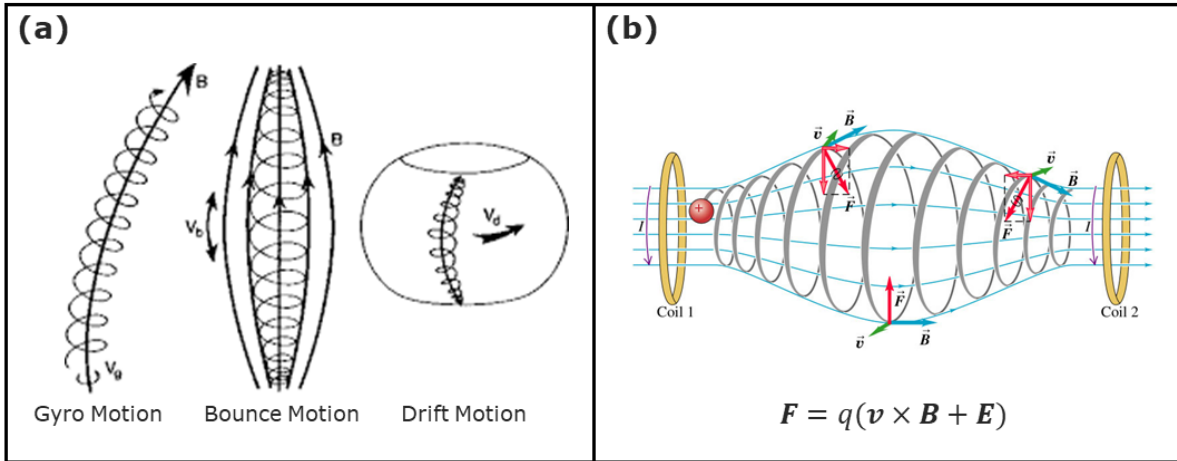
Figure 1. a) Diagram of the 3 primary motions of electrons in the radiation belts; b) Diagram of the Lorentz force (F) causing a charged particle to bounce in a magnetic bottle. Although the charge of the particle is positive in the diagram, electrons have negative charges which would result in counterclockwise gyro motion around the magnetic field lines rather than clockwise motion. The direction of the Lorentz force causes the electron velocity vector (pitch angle) to pitch toward the region of lower magnetic field strength in the center of the bottle. Figure a) from Ng et al. (2013); Figure b) from Physics Stack Exchange.

field line as it transitions from moving toward the atmosphere to moving away from the atmosphere. Electron pitch angle refers to the angle between the velocity vector of an electron and the local magnetic field line. Electrons with mirror points located below 100km altitude (an approximation of the boundary of the atmosphere) will likely ionize molecules in the upper atmosphere before bouncing back into the radiation belts. These electrons are considered as part of the precipitating population. Electrons with mirror points located above the 100km altitude limit will bounce before reaching the upper atmosphere. These electrons will continue bouncing periodically and are considered as part of the trapped population.

Electrons with more perpendicular equatorial pitch angles are more easily bounced before precipitating into the atmosphere and are therefore more likely to be trapped in the radiation belts. Electrons with more parallel equatorial pitch angles are more likely to precipitate into the upper atmosphere before bouncing. The range of equatorial pitch angles that result in precipitation within one bounce is called the bounce loss cone (BLC), which typically ranges from 0 degrees to an upper limit of ~10 degrees depending on the altitude and energy of the electron population. Figure 2 provides a visualization of electron bounce motion, mirror points, and the BLC.

Electron precipitation is widely known as an essential loss process from the Earth's radiation belts into the upper atmosphere. While there have been many recent studies on the space weather phenomena that cause electron precipitation, characteristics of electron microbursts are still relatively unknown. First observed in 1964 (Anderson & Milton 1964), microbursts have been found to occur primarily in the 2-10 magnetic local time (MLT) region and in the 3-8 L-Shell range (Douma et al. 2017). Microburst events are sub-second enhancements of MeV-energy electrons observed in the high latitude regions of the inner magnetosphere. It is well established that microbursts are the results of pitch angle scattering mechanisms which fill the bounce loss cone (BLC) and cause electrons to precipitate into the upper atmosphere.

In general, microbursts are associated with whistler mode chorus wave activity in the morning MLT region (Lorentzen et al. 2001a)(O'Brien et al. 2003)(Mozer et al. 2018). It has previously been theorized that microbursts are generated when electrons resonate with plasma waves in the magnetosphere, and recent models studying particle-wave physics have shown that it is possible for microbursts to be generated from resonant interactions between chorus plasma waves and relativistic electrons (Saito et al. 2012). Douma et al. (2017) have suggested that EMIC plasma waves may also play a role in microburst generation in the 13-22 MLT region. Meredith et al. (2014) have found that most EMIC waves occur in the 4-7 L-Shell range, and Usanova et al. (2012) suggest that EMIC waves driven by solar wind compression at the initial onset of moderate geomagnetic storms likely occur at > 6 L-Shell values. Although there have been links between microburst occurrence and EMIC wave activity, stronger correlations between microburst occurrence
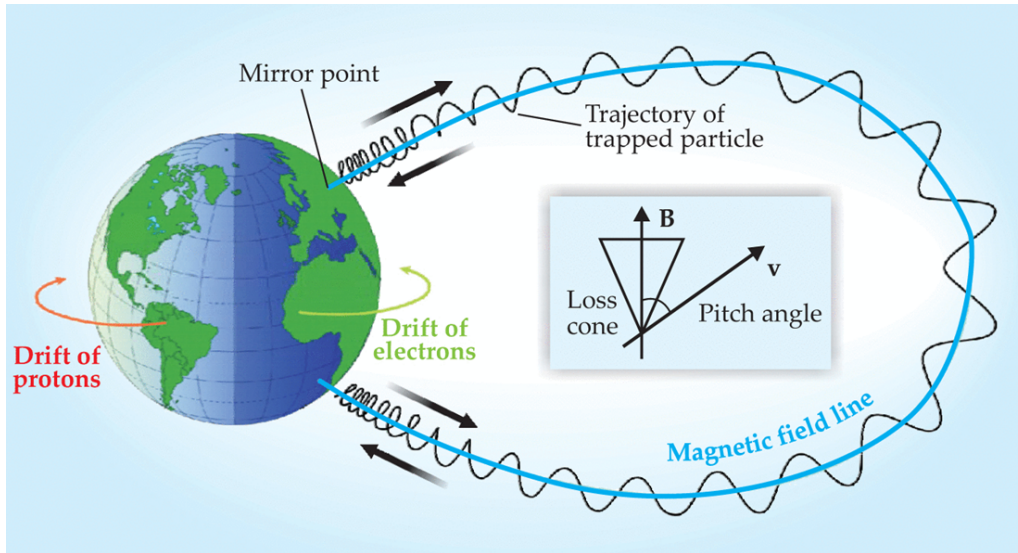
Figure 2. Upper hemisphere and lower hemisphere electron mirror points are shown for a single electron undergoing bounce motion. In the center of the diagram, a visualization of electron pitch angle and the BLC is provided. Although the BLC appears as a 2-dimensional triangle in the diagram, the BLC is a 3-dimensional cone of pitch angles that would result in precipitation. This cone is symmetric around the local magnetic field line. Figure from Day (2008).

and VLF wave amplitude and frequency point to chorus waves as the primary source of microbursts (Douma et al. 2018).

Geomagnetic storm activity is thought to be the underlying cause of plasma wave-induced microburst activity, although there is still debate regarding when peak electron loss rates occur. Blum et al. (2015) used a superposed epoch analysis of multiple geomagnetic storms to show an increase in microburst flux magnitude and occurrence at the initial onset of storms. More recently, Douma et al. (2019) have found that microburst flux magnitude increases with increasing AE index intensity. While some studies show that electron loss rates peak in the main phase of geomagnetic storms (O'Brien et al. 2004)(Tu et al. 2010), others indicate that peaks in microburst flux magnitude and associated electron loss rates occur in the recovery phase (Lorentzen et al. 2001b).

In previous studies, microburst associated electron loss rates have been estimated; however, the pitch angle distributions were assumed to be fully isotropic (Lorentzen et al. 2001b). Although these results have provided essential information regarding global electron loss rates from the radiation belts, an electron population pitch angle isotropy value could be applied to calculations of total loss rates to increase accuracy. Blake et al. (1996) discusses the potential for theoretical isotropy measurements using differential electron count rates from the HILT instrument onboard the SAMPEX satellite. In this study, we expand on the discussion in Blake et al. (1996) to calculate a qualitative isotropy index value. With this isotropy index, we then calculate the isotropy of microbursts occurring throughout the year 1993 and analyze the spatial, temporal, and flux magnitude dependencies of microburst pitch angle isotropy in the Earth's radiation belts.

2. HILT OBSERVATIONS

The SAMPEX satellite, originally launched from Lompoc, CA on July 3, 1992, was designed to detect energetic electrons and ions in Earth's radiation belts. The spacecraft orbited in a near-polar low Earth orbit (LEO) at an altitude of ˜500-700km (Baker et al. 1993).

The HILT instrument, onboard the SAMPEX satellite, was composed of a 4x4 array of $10cm^2$ solid-state SiLi detectors which were grouped into four rows of four detectors. Each detector row recorded $> 1MeV$ electron counts at a time resolution of 100ms. The field of view constrained by the instrument aperture was 68 degrees by 68 degrees (Blake et al. 1996)(Mason et al. 1998).

The view of each individual detector row was slightly different from the other rows due to the geometry of the detector array, which caused each row to measure slightly different electron counts based on the distribution of electron pitch angles. Electron populations in the radiation belts can range from highly isotropic to highly anisotropic pitch angle distributions. Isotropic distributions are populations of electrons with evenly scattered pitch angles. In an isotropic

distribution, there is an equal amount of perpendicular pitch angles and parallel pitch angles. Anisotropic distributions are populations of electrons with unevenly scattered pitch angles. Typically, anisotropic distributions in the radiation belts are composed mostly of perpendicular pitch angles and very few parallel pitch angles. Generally, in isotropic distributions the BLC is full and in anisotropic distributions the BLC is less full. Since electron precipitation occurs when the BLC is full of electrons with parallel pitch angles, high isotropy distributions result in more direct electron precipitation into the upper atmosphere. Conversely, low isotropy distributions result in less electron precipitation. Example pitch angle distributions are shown in Figure 3.
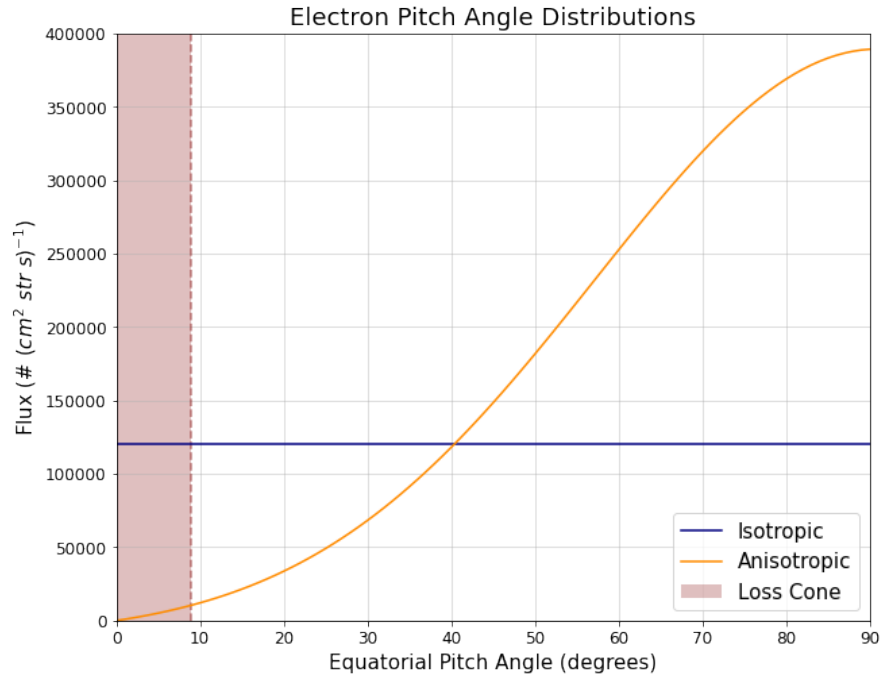
Figure 3. Example isotropic (blue) and anisotropic (orange) electron pitch angle distributions found in the inner magnetosphere. The BLC is indicated by the red shaded region. As shown above, the isotropic distribution fills the BLC while the anisotropic distribution is populated by pitch angles larger than those within the BLC region.

A spacecraft pitch angle filter of less than 40 degrees with respect to the local magnetic field lines was used for all data in the following sections. A large majority of the microbursts detected in 1993 were observed while the spacecraft was angled at 40 degrees or less, which is why this spacecraft pitch angle filter was chosen.

If all HILT detector rows count the same number of energetic electrons, the electron distribution is isotropic. If there is a large differential in counts across the detector rows, the electron distribution is anisotropic. When the angle between the boresight and the local magnetic field line is around 40 degrees or less, a qualitative measurement of pitch angle isotropy can be determined for an electron population. By taking the ratio of electron counts between solid-state detector row 1 (SSD1) and solid-state detector row 4 (SSD4), the isotropy index is calculated as shown in Equation (1):

$$I = N_{100,min}/N_{100,max} \tag{1}$$

Where I is the isotropy index (on a 0 to 1 scale), N_{100} is the number of electrons in 100ms, $N_{100,min}$ is the N_{100} value from the detector row with lower counts, and $N_{100,max}$ is the N_{100} value from the detector with higher counts. In this context, an I value approaching 0 indicates a highly anisotropic population and an I value approaching 1 indicates a highly isotropic population. To visualize the significance of the isotropy index, plots of SSD1 flux, SSD4 flux, and isotropy index versus time are shown in Figure 4. Microburst events are observed as rapid spikes in SSD1 and SSD4 flux. Note that during microburst events the two row fluxes spike up to relatively equal levels (more isotropic) and during quiet times the two row fluxes return to consistent but unequal values (less isotropic). Throughout this study,

we will compare pitch angle isotropy during microbursts with pitch angle isotropy during non-microburst times, which will be referred to as the background population.
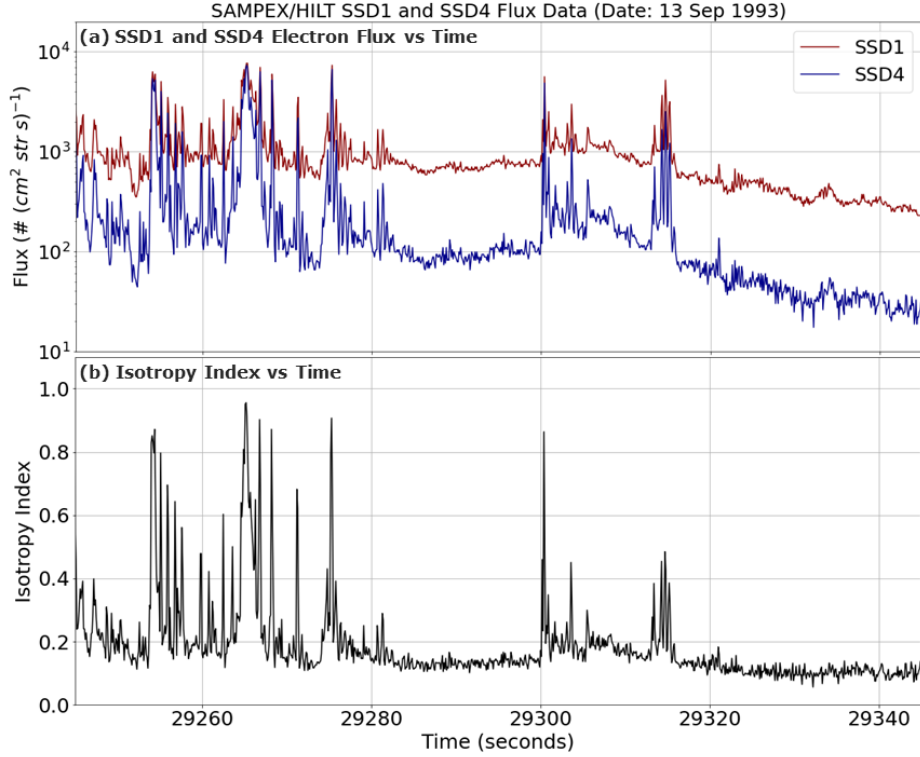
Figure 4. a) Electron flux from SSD1 (red) and SSD4 (blue) rows vs time. b) Isotropy index vs time. Rapid increases in row flux rates indicate when microbursts occur, and flat row flux rates indicate when microbursts are not occurring (referred to as the background population). During microburst events, isotropy index spikes close to 1 then returns to low values of ~0.1 during quiet times.

To begin the analysis of the correlation between microburst events and increased pitch angle isotropy, we used a microburst detection algorithm developed by O'Brien et al. (2003):

$$(N_{100} - A_{500})/\sqrt{1 + A_{500}} > 50 \tag{2}$$

Where N_{100} is the number of electrons in 100ms and A_{500} is the centered rolling average of N_{100} over a 500ms time interval. This algorithm effectively detects rapid enhancements of electrons by measuring how much the electron count rates deviate from a rolling average. For our analysis of microburst flux magnitude, we applied the microburst flux magnitude formula used in Blum et al. (2015):

$$M = N_{100} - B_{3000} \tag{3}$$

Where M is the microburst flux magnitude and B_{3000} is the centered rolling 10th percentile of N_{100} over a 3-second time interval. This provides the relative intensity of the microburst above the background flux levels.

3. RESULTS

To determine the spatial and temporal dependence of microburst isotropy in the inner magnetosphere, the study was conducted in two parts. In Section 3.1, correlations between microburst isotropy, magnitude, MLT, and L-shell over the year 1993 were observed. In Section 3.2, a superposed epoch analysis of the variation of microburst isotropy with respect to storm phases was conducted for 6 intense geomagnetic storms that fit a typical Dst profile.

3.1. Statistical Study

First we explore the dependence of microburst isotropy with microburst intensity by plotting microburst isotropy with respect to microburst flux magnitude. A 2-dimensional histogram of this trend is plotted in Figure 5.
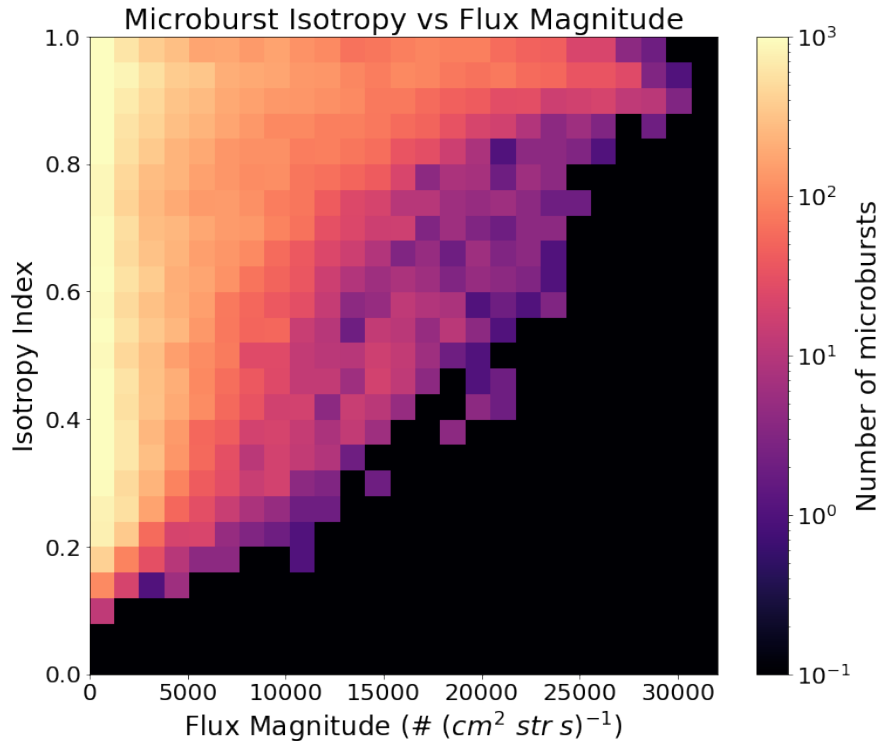
Figure 5. 2D histogram of microburst isotropy index vs microburst flux magnitude using data from the year 1993. Due to the logarithmic scaling of the colorbar, any zero value pixel was altered to a 10^{-1} value to plot correctly in the figure. At low flux magnitudes, microbursts are observed at a wide range of isotropy indices. At high flux magnitudes, microbursts are observed to be highly isotropic.

With isotropy index plotted on the y-axis and flux magnitude plotted on the x-axis, the colorbar indicates the number of microbursts observed at each respective isotropy-magnitude coordinate. Due to the exponential decay of microburst counts as magnitude increases, the colorbar was scaled logarithmically.

Results from this analysis show that for low flux magnitudes there is a wide spread in microburst isotropy index ranging from 0.1 to 1. As magnitude increases towards the upper limit of ~30,000 electrons (cm^2 str s)$^{-1}$, low isotropy values drop out and only high isotropy microbursts are observed. This would indicate that high flux magnitude microbursts result in significant electron precipitation into the atmosphere and low magnitude microbursts have varying degrees of impact on electron precipitation.

To analyze the spatial dependence of microburst isotropy within the radiation belts, occurrence distributions and isotropy values vs MLT-L were plotted in Figure 6.

Panels a) and b) are dial plots of microburst occurrence and background sampling rates throughout the year 1993. As shown previously, microbursts most often occur in the morning magnetic local time region (which these results agree with). The background sampling distribution shows good coverage of MLT and L-Shell values throughout the orbit of the SAMPEX spacecraft during the time period used in this study.

Panels c) and d) are dial plots of the median microburst and background isotropy index for each respective MLT-L bin. To eliminate any orbit effects, we compare relative isotropy of microbursts with the background population. By taking the difference between plots c) and d), the microburst isotropy relative to the background population is examined, which is plotted in Figure 7.

From Figure 7, it can be determined that the largest difference in isotropy occurs in the evening magnetic local time region and the lowest difference occurs at noon. It is important to note that the peak isotropy difference in the evening
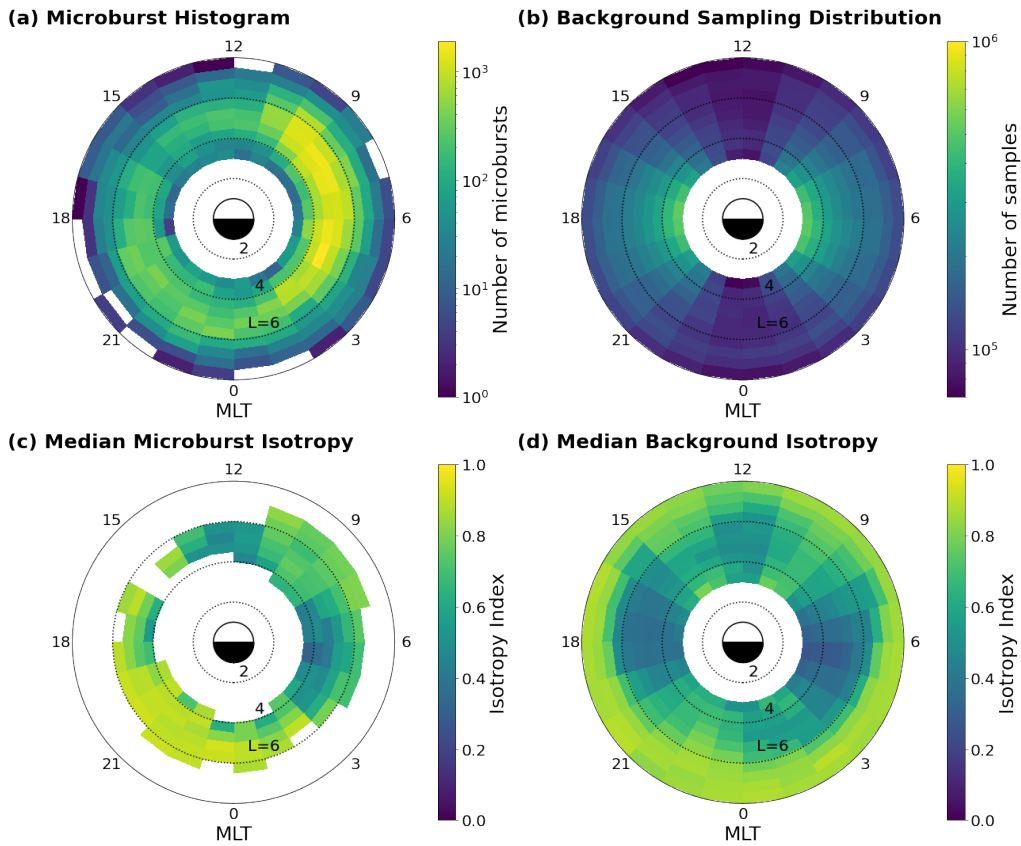
Figure 6. a) Dial plot (histogram) of microburst occurrence; b) Dial plot (histogram) of the background sampling distribution; c) Dial plot of median microburst isotropy; d) Dial plot of median background isotropy. All panels use data from the year 1993 and are plotted as a function of MLT and L-Shell.
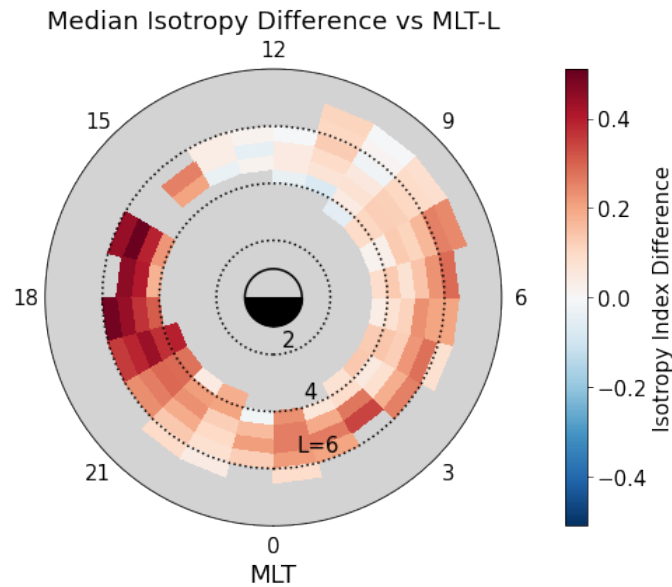
Figure 7. Dial plot of the difference in isotropy index between microbursts and the background population as a function of MLT and L-Shell in the year 1993. Red regions indicate where microbursts are more isotropic than the background population, white regions indicate zero difference, and blue regions indicate where microbursts are less isotropic than the background population.

MLT regions is due to the high microburst isotropy index values seen in Figure 6c. This indicates that, although microbursts are most frequent in the morning MLT region, individual microbursts are on average more isotropic in the evening.

3.2. *Storm-time Analysis*

To analyze the storm-time dependence of microburst isotropy during geomagnetic storms, we use the Disturbance Storm-time (Dst) index to define geomagnetic storm phases. The Dst index is a ground-based data set which measures the hourly disturbance of the global ring current at equatorial latitudes. By recording the Dst fluctuations during geomagnetic storms, the relative strength and time evolution of individual storms can be determined.

Out of 9 intense storms in the year 1993 with $Dst_{min} <$ -100nT, 6 storms with typical Dst profiles were selected. Table 1 details the start and end dates of each storm in addition to MLT-sampling and Dst profile information. Due to the near-polar orbit of the spacecraft, SAMPEX primarily sampled MLT values on opposite sides of the earth for each individual storm (ie. 12 and 24 MLT). Figure 8 shows Dst index vs time throughout the duration of each storm.

**Table 1.** List of intense geomagnetic storms selected from 1993

Time of Dst_{min}	Event Start	Event End	Notes
Feb 17, UT 14	Feb 16	Feb 23	MLT: 12-24; Dst_{min}: -103 nT
Mar 09, UT 06	Mar 08	Mar 11	MLT: 09-21; Dst_{min}: -145 nT
Mar 11, UT 18	Mar 11	Mar 13	MLT: 08-20; Dst_{min}: -124 nT
Apr 05, UT 06	Apr 03	Apr 10	MLT: 05-17; Dst_{min}: -191 nT
Sep 13, UT 06	Sep 11	Sep 18	MLT: 07-19; Dst_{min}: -189 nT
Nov 04, UT 06	Nov 02	Nov 09	MLT: 12-24; Dst_{min}: -127 nT
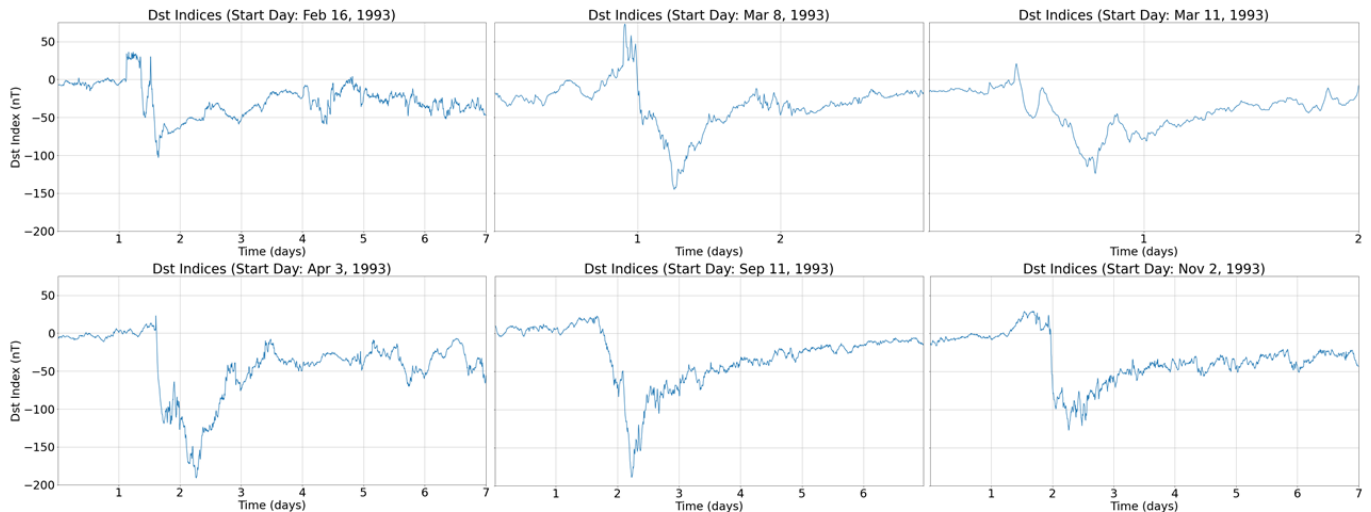
Figure 8. Dst profiles of the 6 storms selected for analysis

Generally, geomagnetic storms are separated into three distinct phases: initial phase, main phase, and recovery phase. The initial phase of a geomagnetic storm is defined as the region from the initial increase in Dst index to the maximum Dst index. The main phase is defined as the region of time from when the Dst is at a local maximum to when it is at a local minimum during the storm. The recovery phase is defined as the region of time after the Dst minimum in which the Dst index slowly recovers and returns to values near 0 nT.

To analyze how microburst isotropy varies with storm phase, we used the above criteria to determine the storm phase boundaries during each individual storm and binned isotropy measurements by storm phase. A superposed epoch study was then conducted by taking the median isotropy index of all microbursts and background for each of the three storm phases, which can be observed in Figure 9.
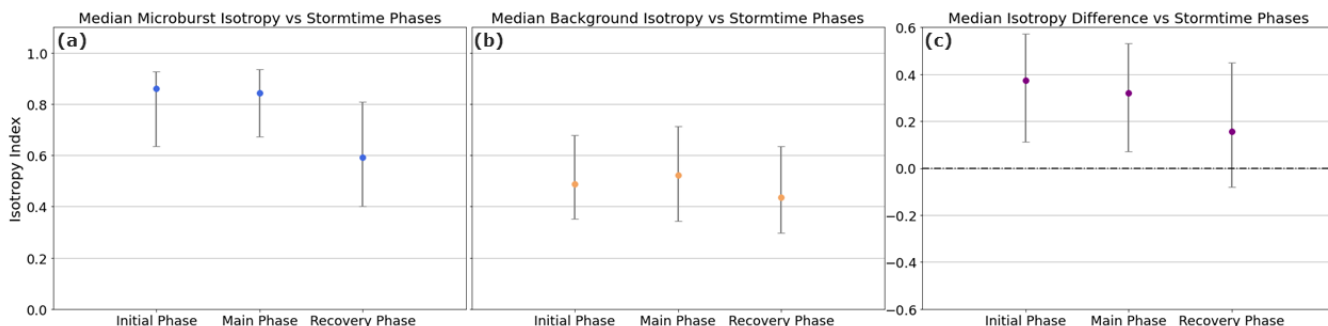
Figure 9. Dst storm-time analysis: a) plot of median microburst isotropy vs storm-time phases; b) plot of median background isotropy vs storm-time phases; c) plot of median isotropy difference vs storm-time phases. Upper limit and lower limit error bars indicate 25th and 75th percentiles, respectively.

Similarly to Section 3.1, by taking the difference between plots a) and b), the storm-time dependence of microburst isotropy relative to the background population can be determined in plot c). While the median background isotropy remains fairly even throughout initial and main phases, the median microburst isotropy changes to lower values during the recovery phase. Results of this epoch study indicate that microburst isotropy relative to the background population is highest at the initial onset of intense geomagnetic storms, remains relatively constant through the main phase, and drops substantially as storms progress into the recovery phase.

4. DISCUSSION

In the context of previous electron precipitation research, this study provides information that will allow for a more accurate calculation of electron loss rates into the upper atmosphere. In Section 3.1, we have shown that the microburst isotropy index is positively correlated with microburst flux magnitude. Based on the theory that isotropic microbursts fill the BLC and therefore increase electron precipitation, this indicates that more intense microbursts also result in more precipitation. Although past papers have found correlations between microburst flux magnitude and geomagnetic activity, this is the first result showing a positive correlation between microburst isotropy and microburst flux magnitude. This finding provides the potential for future studies to more accurately quantify the effects of individual microbursts with specific flux magnitudes. In previous studies, full isotropy was assumed to calculate electron loss rates. Now, pitch angle isotropy can be considered using this isotropy-magnitude trend.

Results from Section 3.1 also suggest that the electron pitch angle diffusion of microbursts generated in the evening MLT region may be more effective than in other MLT regions. For example, in Figure 7 it is apparent that microbursts occurring in the 4-6 L-shell and 16-20 MLT region are more isotropic relative to the background population compared to morning-side microbursts. This indicates that for individual microburst events in the evening MLT region, electron pitch angles are more effectively scattered into the BLC. EMIC wave activity is known to occur in the noon and evening MLT regions, which could indicate that these more isotropic microbursts may be caused by EMIC waves rather than chorus waves (more often observed on the morning side). While the general consensus is that chorus waves are much closer linked to microburst activity, our results indicate that the rare cases of EMIC wave driven microbursts found by Douma et al. (2018) may be more isotropic than microbursts generated by chorus wave activity. Further studies must be conducted to establish a more substantial link between microburst isotropy and the wave mode producing microbursts in different MLT regions.

In Section 3.2, we found that the microburst isotropy index was highest in the initial and main phases and dropped during the recovery phase of intense geomagnetic storms. Although Lorentzen et al. (2001b) have found that microbursts are most intense and cause more precipitation in the recovery phase, our results are in partial agreement with the findings O'Brien et al. (2004) and Tu et al. (2010) that indicate electron loss due to microbursts peaks in the main phase. Past papers studying peak electron loss rates have been focused on various types of geomagnetic storms, which could explain the slight deviation of our results with past findings. Similar studies focused on small or moderate geomagnetic storms could be accomplished using techniques detailed in this paper.

Lastly, it is important to note that microbursts were found to be more isotropic than the background population in each section of the study. While this was expected, it supports the fundamental idea that microburst events in the

Earth's magnetosphere contribute to electron precipitation by means of a rapid pitch angle scattering mechanism that fills the BLC. These findings also reveal that, while microbursts are generally more isotropic than the background, there is a great deal of variability in isotropy between individual microbursts. from By finding a qualitative measurement of microburst pitch angle isotropy, we have developed a new tool for understanding when and where microbursts most effectively fill the BLC and impact electron loss rates from the radiation belts.

5. SUMMARY

In this study, we use a combination of SAMPEX/HILT electron measurements and ground-based Dst index measurements from the year 1993 to characterize pitch angle distributions of MeV-energy electrons. In the first part of Section 3.1, we compared microburst isotropy index with microburst flux magnitude. In the second part of Section 3.1, we looked at the variation of microburst and background isotropy versus MLT and L-Shell. In Section 3.2, we looked at the storm-time dependence of microburst and background isotropy during intense geomagnetic storms. Our results can be summarized by the following points:

1. Microburst isotropy is strongly correlated with microburst flux magnitude. At low microburst magnitudes, the isotropy index was widely varying; spanning from values of 0.1 to 1 isotropy index. At high microburst magnitudes, the microburst isotropy index converged on the upper limit of 1.

2. Similar to previous studies, we found that microbursts were most frequent in the morning MLT region. The microburst isotropy index compared to the background population was highest in the evening magnetic local time region and lowest in the noon region.

3. Microburst isotropy compared to the background population was found to be highest in the initial and main phases of geomagnetic storms and lowest in the recovery phase. This result suggests that microbursts more effectively scatter electrons into the BLC during the initial onset and main phase of intense geomagnetic storms.

4. Throughout the study, microburst isotropy was higher than the background isotropy. This finding supports the theory that microburst events act as rapid pitch angle scattering mechanisms that fill the BLC causing increased electron precipitation.

REFERENCES

Anderson, K. A., & Milton, D. W. 1964, J. Geophys. Res., 69, 4457, doi: 10.1029/JZ069i021p04457

Baker, D. N., Mason, G. M., Figueroa, O., et al. 1993, IEEE Transactions on Geoscience and Remote Sensing, 31, 531, doi: 10.1109/36.225519

Blake, J. B., Looper, M. D., Baker, D. N., et al. 1996, Advances in Space Research, 18, 171

Blum, L., Li, X., & Denton, M. 2015, Journal of Geophysical Research (Space Physics), 120, 3783, doi: 10.1002/2014JA020633

Day, C. 2008, Physics Today, 61, 18, doi: 10.1063/1.2970203

Douma, E., Rodger, C. J., Blum, L. W., & Clilverd, M. A. 2017, Journal of Geophysical Research (Space Physics), 122, 8096, doi: 10.1002/2017JA024067

Douma, E., Rodger, C. J., Blum, L. W., et al. 2019, Journal of Geophysical Research (Space Physics), 124, 5627, doi: 10.1029/2019JA026757

Douma, E., Rodger, C. J., Clilverd, M. A., et al. 2018, Journal of Geophysical Research (Space Physics), 123, 1279, doi: 10.1002/2017JA024754

Lorentzen, K. R., Blake, J. B., Inan, U. S., & Bortnik, J. 2001a, J. Geophys. Res., 106, 6017, doi: 10.1029/2000JA003018

Lorentzen, K. R., Looper, M. D., & Blake, J. B. 2001b, Geophys. Res. Lett., 28, 2573, doi: 10.1029/2001GL012926

Mason, G. M., Baker, D. N., Blake, J. B., et al. 1998, in 1998 IEEE Aerospace Conference, Vol. 5, Vol. 5, 389–412

Meredith, N. P., Horne, R. B., Kersten, T., Fraser, B. J., & Grew, R. S. 2014, Journal of Geophysical Research (Space Physics), 119, 5328, doi: 10.1002/2014JA020064

Mozer, F. S., Agapitov, O. V., Blake, J. B., & Vasko, I. Y. 2018, Geophys. Res. Lett., 45, 511, doi: 10.1002/2017GL076120

Ng, Y., Hoshino, M., Amano, T., Shirakawa, K., & Higashimori, K. 2013, Semantic Scholar

O'Brien, T. P., Looper, M. D., & Blake, J. B. 2004, Geophys. Res. Lett., 31, L04802, doi: 10.1029/2003GL018621

O'Brien, T. P., Lorentzen, K. R., Mann, I. R., et al. 2003, Journal of Geophysical Research (Space Physics), 108, 1329, doi: 10.1029/2002JA009784

Saito, S., Miyoshi, Y., & Seki, K. 2012, Journal of Geophysical Research (Space Physics), 117, A10206, doi: 10.1029/2012JA018020

Tu, W., Selesnick, R., Li, X., & Looper, M. 2010, Journal of Geophysical Research (Space Physics), 115, A07210, doi: 10.1029/2009JA014949

Usanova, M. E., Mann, I. R., Bortnik, J., Shao, L., & Angelopoulos, V. 2012, Journal of Geophysical Research (Space Physics), 117, A10218, doi: 10.1029/2012JA018049